N-methylacetamide (NMA) to the extent of ~1.5%.[2] The latter value is consistent with the energy difference between NMA isomers obtained from temperature-dependent matrix-isolation studies[3] (~2.3 kcal/mol) and from ab initio calculations[2,4] (~2.5 kcal/mol). Recent resonance Raman studies under conditions of high laser pulse energies[5,6] indicate that *trans*-NMA can be photoisomerized to *cis*-NMA, the argument being based in part on a proposed assignment of the amide II mode of the cis peptide group. It is therefore important to have a detailed understanding of the vibrational dynamics of this group. A previous normal-mode analysis of *cis*-NMA[3] was based on the assumption that its force field and internal geometry are the same as those of *trans*-NMA, which may not be warranted. We have computed the ab initio geometry and force field of *cis*-NMA, both the isolated molecule and with two H_2O molecules hydrogen bonded to it, and have obtained its normal modes. These confirm the assignment made in the resonance Raman studies,[5,6] but give significantly different normal modes than predicted by the previous analysis.[3]

The geometry of isolated *cis*-NMA was obtained at the Hartree-Fock level with five different basis sets: 3-21G*, 4-31G, 4-31G*, 6-31G, and 6-31G*. The four possible conformations with respect to CH_3 group rotations were completely optimized, and it was found that the order of stability is the same for all the basis sets. The most stable structure has a *C*-methyl H eclipsing the O and an *N*-methyl H eclipsing the (N)H, which differs from that assumed in the earlier normal-mode calculation[3] but is the same as that found in another ab initio study.[4] The bond lengths are very close to those of the most stable form of *trans*-NMA, for which we also optimized the four conformations[7] (the most stable trans structure has the same local eclipsed conformations as the cis). The bond angles, however, are more variable, some differing by 5-6° between the two structures.

Force fields were calculated with the 4-31G* and 6-31G* basis sets, and normal modes obtained from each set were compared. The frequencies and modes are essentially the same, and we therefore based all our results on the 4-31G* calculations. Since reliable eigenvectors depend on having accurate force constants, and since the ab initio values are generally high by 10-20% for such basis sets,[8] we chose to scale the force constants to experimental frequencies. Scale factors were obtained by optimizing the force constants for *trans*-NMA to its matrix-isolated frequencies[7] and then transferring these 10 scale factors to the ab initio force field of *cis*-NMA. Good agreement with experiment[3] required the modification of only one scale factor, that for CN stretch (s) being changed from 0.74 to 0.84. These scale factors were then transferred unchanged to the hydrogen-bonded *cis*-NMA system.

The effects of aqueous hydrogen bonds in modifying the normal modes of a *cis*-NMA molecule should be satisfactorily modeled by a complex that involves only the C=O and NH groups in interactions with water molecules. Although some ab initio energy studies[9-11] have examined formamide complexed with several such H_2O molecules, we feel that the cluster number and geometry are not critical and that the predominant effects on the normal modes are revealed by the presence of two H_2O molecules, one bonded to each group. We have therefore obtained the geometry and force field by the total optimization of such a *cis*-NMA-$(H_2O)_2$ complex.

The results of the calculations on isolated and hydrogen-bonded NMA are shown in Table I for the main amide and skeletal modes and are compared with experimental data for matrix-isolated[3] and aqueous[6] *cis*-NMA, respectively. We see that the amide II mode of the hydrogen-bonded molecule is predicted near the observed value of 1496 cm^{-1} [5,6] and is mainly CN s with no NH in-plane bend (ib) (≥10), consistent with experimental evidence.[6] This mode is significantly different in the isolated molecule, although it still contains no NH ib, in distinction to this coordinate being the largest contributor in an earlier calculation.[3] Other modes are also affected by hydrogen bonding, but to different degrees. Amide I, near 1650 cm^{-1}, can involve an HOH bend, although the extent is very sensitive to the scale factor for the latter force constant. These differences in modes, as well as in frequencies, are undoubtedly due to the significant changes in force constants that occur on hydrogen bonding; e.g., CN s, 8.1%; CO s, -8.3%; CO ib, 13.5%; NH ib, 46.7%; NH out-of-plane bend, 54.1%; CN s, NH ib, 94.8%. These changes are evaluated elsewhere in greater detail,[12] but it is clear that isolated molecules may not be adequate models for the normal modes of molecules that interact strongly with solvent.

Table I. Amide and Skeletal Modes of Isolated and Aqueous Hydrogen-Bonded *cis*-NMA

ν(obsd)[a]	ν(calcd)	potential energy distribution[b]
1707	1717	CO s (78), CCN d (12)
~1650	1645	CO s (28), HOH sb (50)
1485	1481	NCH_3 ab (54), CN s (16), NCH_3 r (14)
1496	1499	CN s (33), CC s (11), NCH_3 ab (10)
1325	1331	CCH_3 sb (51), CN s (17), NH ib (12), CO ib (12)
1316	1354	CCH_3 sb (63), CN s (11)
	798	CC s (52), CN s (20), NC s (10)
821	808	CC s (58), CN s (20), NC s (11)
	516	CN t (36), CO ob (26), NH ob (17), CCH_3 r (13)
	678	CN t (33), CO ob (29), NH ob (21), CCH_3 r (13)

[a] Top line: matrix isolated.[3] Bottom line: aqueous solution.[6] [b] s = stretch, d = deformation, t = torsion, ab = antisymmetric bend, sb = symmetric bend, ib = in-plane bend, ob = out-of-plane bend. Contributions ≥10.

Acknowledgment. This research was supported by NSF Grants DMB-8816756 and DMR-8806975.

(2) Radzicka, A.; Pedersen, L.; Wolfenden, R. *Biochemistry* **1988**, *27*, 4538-4541.
(3) Ataka, S.; Takeuchi, H.; Tasumi, M. *J. Mol. Struct.* **1984**, *113*, 147-160.
(4) Jorgensen, W. L.; Gao, J. *J. Am. Chem. Soc.* **1988**, *110*, 4212-4216.
(5) Wang, Y.; Purrello, R.; Spiro, T. G. *J. Am. Chem. Soc.* **1989**, *111*, 8274-8276.
(6) Song, S.; Asher, S. A.; Krimm, S.; Shaw, K. D. *J. Am. Chem. Soc.*, in press.
(7) Mirkin, N. G.; Krimm, S. *J. Mol. Struct.*, in press.
(8) Fogarasi, G.; Pulay, P. *Vibrational Spectra and Structure*; Durig, J. R., Ed.; Elsevier: Amsterdam, 1985; pp 125-219.
(9) Johansson, A.; Kollman, P.; Rothenberg, S.; McKelvey, J. *J. Am. Chem. Soc.* **1974**, *96*, 3794-3800.
(10) Del Bene, J. E. *J. Chem. Phys.* **1975**, *62*, 1961-1970.
(11) Hinton, J. F.; Harpool, R. D. *J. Am. Chem. Soc.* **1977**, *99*, 349-353.
(12) Mirkin, N. G.; Krimm, S., to be published.

Dipolar NMR Spectroscopy of Nonoxidic Glasses. Structural Characterization of the System Phosphorus-Selenium by ^{31}P-^{77}Se Spin Echo Double Resonance NMR

D. Lathrop and H. Eckert*

Department of Chemistry
University of California, Santa Barbara
Santa Barbara, California 93106

Received August 2, 1990

In spite of the long-standing importance of non-oxide chalcogenide glasses in infrared optics and semiconductor technology, quantitative concepts describing the structural principles in these systems are just emerging. Recently, unique insights have been obtained via dipolar solid-state NMR techniques.[1]

The binary phosphorus-selenium system forms glasses over a wide compositional region (0-52 atom % P)[2] and is an ideal model system for studies directed at the development of structural concepts for chalcogenide glasses. Previous ^{31}P spin-echo experiments have served to establish the statistics of P-Se vs P-P

(1) Eckert, H. *Angew. Chem.* **1989**, *101*, 1723.
(2) Borisova, Z. U.; Kasatkin, B. E.; Kim, E. I. *Izv. Akad. Nauk SSSR, Neorg. Mater.* **1973**, *9*, 822. Heyder, F.; Linke, D. *Z. Chem.* **1973**, *13*, 480. Blachnik, R.; Hoppe, A. *J. Noncryst. Solids* **1979**, *34*, 191.

0002-7863/90/1512-9017$02.50/0

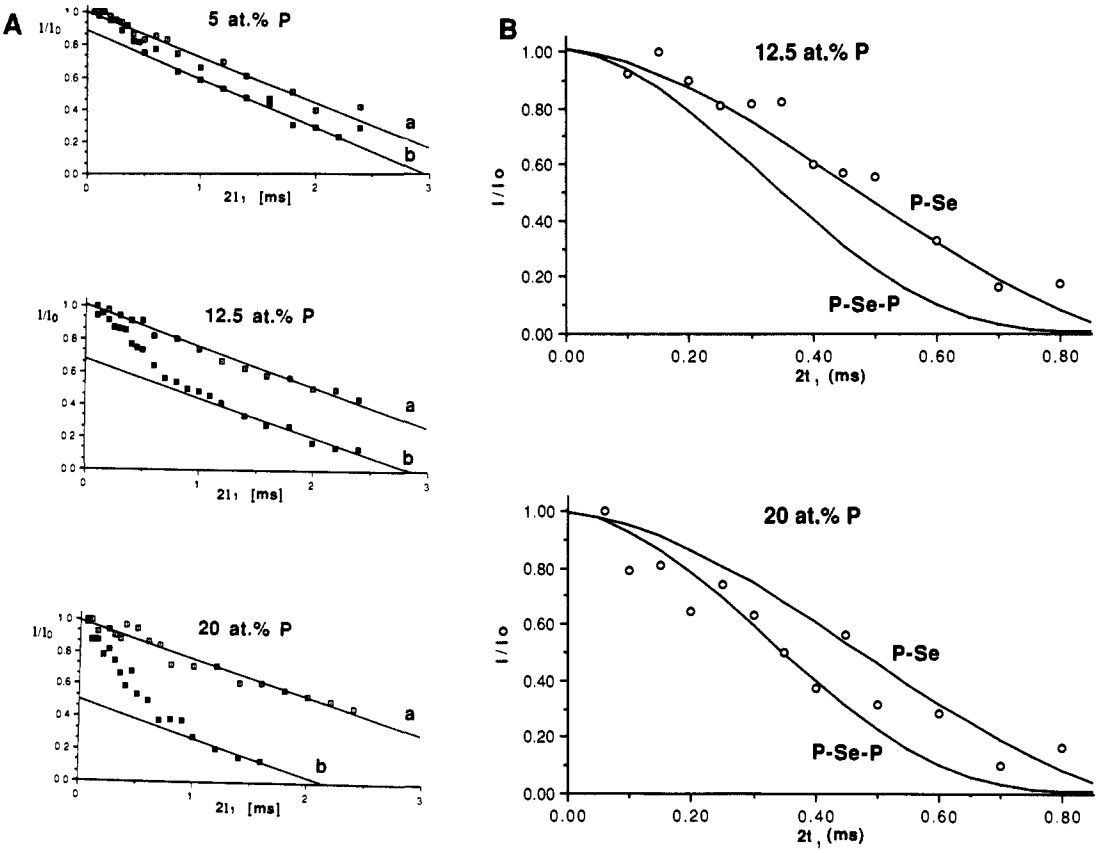

Figure 1. $^{31}P-^{77}Se$ SEDOR results on three P–Se glasses. (A) Normalized ^{77}Se spin-echo intensities as a function of the evolution time $2t_1$ (a) without and (b) with application of the ^{31}P pulse. The straight lines are linear least-squares fits to the whole data of curve a and to the long-term behavior of curve b, respectively. (B) Dipolar decay curves of the P-bonded Se atoms, obtained via SEDOR difference analysis (see text). Top: glass containing 12.5 atom % P. Bottom: glass containing 20 atom % P. The solid curves show the simulated decay within the region 0 ms $\leq 2t_1 \leq$ 0.85 ms for isolated P–Se bonds and P–Se–P bridges, respectively.

bonding in these glasses,[3] Here we report a complementary experiment, which helps to unravel the statistics of Se–Se vs Se–P bonding. This question relates to the issue of whether the P atoms are distributed in an isolated fashion (scenario I) or if there exists a tendency toward phosphorus clustering via preferred formation of P–Se–P bridges (scenario II).[5] Both models differ with respect to the fraction of P-bonded selenium atoms, Se_P, as contrasted to the remaining atoms, Se_{Se}, which are only bonded to other selenium atoms. Assuming all three-coordinate phosphorus, scenario I results in 3.0 Se_P atoms/P atom, whereas scenario II predicts 1.5 Se_P atoms/P atom. This question can be addressed experimentally by $^{31}P-^{77}Se$ spin echo double resonance (SEDOR) spectroscopy.

The methodology of SEDOR has been developed and applied to surfaces by Slichter and co-workers.[5-7] Boyce and Ready have used it to study dopant interactions in amorphous silicon alloys.[8] Generally, however, applications have remained scarce, due to the special demands these experiments pose on spectrometer hardware.[9] To the best of our knowledge, this is the first application of heteronuclear $X-Y$ double resonance experiments to bulk glass structure.

Table I. The Fraction $[Se_P]$ of P-Bonded Se Atoms, as Determined Experimentally and Predicted by Scenarios I and II

atom % P	scenario I	scenario II	expt
5.0	0.16	0.08	0.12
12.5	0.43	0.21	0.33
20.0	0.75	0.38	0.48

In our experiments, ^{77}Se spin echoes are generated ($90°-t_1-180°$ sequence) while the ^{31}P spins are inverted at t_1. As a result, the heteronuclear $^{31}P-^{77}Se$ interaction is no longer refocused, and the magnetization associated with the Se_P species decays according to the $^{31}P-^{77}Se$ dipolar coupling constant, as a function of the incremented evolution period $2t_1$. In contrast, the Se_{Se} species remain unaffected by the ^{31}P pulse.

Figure 1 shows the results for three glass compositions. Even in the absence of the ^{31}P pulse, there is considerable decay of the ^{77}Se spin-echo intensity with $2t_1$, due to direct and indirect $^{77}Se-^{77}Se$ interactions. This decay is approximated equally well by either linear or exponential functions; for simplicity we use the linear fit here. In the presence of the ^{31}P pulse, the spin-echo intensity decreases much more rapidly due to the dipolar decay of the magnetization associated with the Se_P species. At times $2t_1 > 1$ ms, this magnetization has been largely drained, and the residual spin-echo intensity is now mostly due to the Se_{Se} species. Note that the slope of this long-term behavior closely matches the slope seen in the absence of the ^{31}P pulse for the *entire* selenium population. Extrapolation of this straight line to zero time helps to estimate the selenium fractions $[Se_P]$ and $[Se_{Se}]$ (see Table I). Subtraction of this line from the experimental data in Figure 1A affords the Se_P dipolar decay function. Figure 1B contrasts this decay function with simulations for an isolated Se–P bond and a P–Se–P species, respectively. The simulations account for the experimentally observed ^{77}Se T_2 and assume a P–Se distance of 2.30 Å.[10] Figure 1B suggests that at 12.5 atom % P the majority

(3) Lathrop, D.; Eckert, H. *J. Am. Chem. Soc.* **1989**, *111*, 3536.
(4) As shown in Ref 3, no P–P bonding occurs in the glasses studied here.
(5) Makowka, C. D.; Slichter, C. P.; Sinfelt, J. H. *Phys. Rev. Lett.* **1982**, *49*, 379; *Phys. Rev. B* **1985**, *31*, 5663.
(6) Wang, P. K.; Slichter, C. P.; Sinfelt, J. H. *Phys. Rev. Lett.* **1984**, *53*, 82.
(7) Shore, S. E.; Ansermet, J. P.; Slichter, C. P.; Sinfelt, J. H. *Phys. Rev. Lett.* **1987**, *58*, 953.
(8) Boyce, J. B.; Ready, S. E. *Phys. Rev. B* **1988**, *38*, 11008.
(9) For the experimental setup, see: Maxwell, R.; Franke, D.; Lathrop, D.; Eckert, H. *Angew. Chem., Int. Ed. Engl.* **1990**, *29*, 882. Typical experimental parameters were as follows: 90° pulse lengths, 6–8 μs (^{31}P) and 7–10 μs (^{77}Se); recycle delay, 15 min; four scans. Details on the sample preparation are given in ref 3.

of the P-bonded Se atoms are bonded to only one P atom, whereas at 20 atom % P the fraction of P–Se–P units is substantially increased, as expected from probability considerations. Both the results of Table I[11] and the compositional evolution apparent in Figure 1B argue against the cluster models previously suggested for the structure of these glasses.[12] A more detailed interpretation, in conjunction with ^{31}P spin-echo and MAS-NMR studies will be published elsewhere.

The results presented here suggest that heteronuclear "*X–Y*" double resonance experiments have considerable potential for elucidating the structure of inorganic ceramics, semiconductors, and glasses. Further applications to other inorganic systems are currently in progress.

Acknowledgment. Funding by the UCSB Academic Senate and the National Science Foundation (DMR-8913738) is gratefully acknowledged. Acknowledgment is made to the donors of the Petroleum Research Fund, administered by the American Chemical Society, for partial support of this research.

(10) The sparse crystallographic literature on P–Se compounds indicates bond lengths ranging from 2.2 to 2.4 Å. SEDOR studies of such models have been impeded by extremely long ^{77}Se T_1's and other difficulties. However, the ^{113}Cd–^{31}P SEDOR of CdP_2, a model compound with similar spin dynamics, yields a dipolar second moment close to that calculated from the crystal structure.

(11) In spite of the potential errors arising from the back-extrapolation, Table I shows that for all three glasses the Se_P fraction is significantly higher than predicted from the cluster model (scenario II). This result is noteworthy, as incomplete inversion of the ^{31}P nuclei by imperfect 180° pulses would lead to underestimates.

(12) Price, D. L.; Misawa, M.; Susman, S.; Morrison, T. L.; Shenoy, G. K.; Grimsditch, M. *J. Noncryst. Solids* **1984**, *66*, 443.

"Outer-Sphere" Oxidation of Nonconjugated Dienes by Simple Iron(III) Complexes: A New Mechanistic Consideration for Oxidation of Arachidonic Acid by Lipoxygenase

Timothy J. Bill, Sylvia Chen, Robert A. Pascal, Jr., and Jeffrey Schwartz*

Department of Chemistry, Princeton University
Princeton, New Jersey 08544-1009

Received June 11, 1990

The design of effective inhibitors of the lipoxygenases, critical enzymes for the biosynthesis of medically important eicosanoids from arachidonic acid,[1] would be abetted by knowledge of the catalytic mechanism(s) of these non-heme iron dioxygenases.[2] Recent mechanistic proposals for this enzymatic reaction have centered on "inner-sphere" oxidation, invoking first an Fe(III)–olefin complex and then an organoiron intermediate.[3] However, "outer-sphere" oxidation of arenes[4] and olefins[5] by simple iron complexes has been observed, suggesting that dienes, too, might be oxidized by a noncoordinative process, one that should be kinetically enhanced by structural factors that favor one-electron oxidation of a double bond. For a 1,4-diene, oxidation should be facilitated by structural effects that maximize π interactions between the formally unconjugated double bonds. For example, arachidonic acid, conformationally constrained through enzyme binding to provide maximum π interaction between Δ^5 and Δ^8 of the tetraene ("homoconjugation"), might undergo facile noncoordinative oxidation. We report that simple 1,4-dienes, "conformationally locked" by incorporation into a ring, are in fact oxidized by simple Fe(III) complexes in a process fully consistent with outer-sphere oxidation in which interaction between the formally nonconjugated double bonds is clearly indicated.

Scheme I

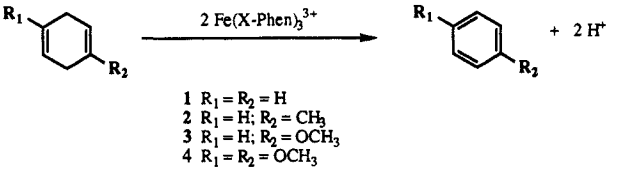

1 $R_1 = R_2 = H$
2 $R_1 = H$; $R_2 = CH_3$
3 $R_1 = H$; $R_2 = OCH_3$
4 $R_1 = R_2 = OCH_3$

Table I. Rates for Oxidation of Dienes by $Fe(X\text{-phen})_3^{3+}$ Complexes

complex[a]	T, °C	olefin[a]	k_2,[b] s^{-1} M^{-1}	rel rate
$Fe(phen)_3^{3+}$	+23	1,4-CHD (**1**)	5.2 (1.0) × 10^{-4}	1.0
	+23	1,3-CHD	9.2 (1.9)	1.8 × 10^4
	+23	1-Me-1,4-CHD (**2**)	4.3 (0.7) × 10^{-3}	8.2
$Fe(phen)_3^{3+}$	−30	1-Me-1,4-CHD (**2**)	4.3 (1.6) × 10^{-4}	1.0
	−30	1-MeO-1,4-CHD (**3**)	0.28 (0.07)	6.6 × 10^2
$Fe(4,7\text{-}Ph_2\text{-}phen)_3^{3+}$	−30	1-MeO-1,4-CHD (**3**)	2.3 (0.9) × 10^{-3}	1.0
	−30	1,4-$(MeO)_2$-1,4-CHD (**4**)	3.7 (1.7) × 10^1	1.6 × 10^4

[a] Phen = 1,10-phenanthroline; CHD = cyclohexadiene. [b] Standard deviations in parentheses.

Table II. Oxidation of 1-Me-1,4-CHD (**2**) by Fe(III) Complexes of Varying Reduction Potential

complex	$E_{1/2}$,[a] V	k_2,[b] s^{-1} M^{-1}	rel rate
$Fe(5\text{-}NO_2\text{-}phen)_3^{3+}$	1.18	1.2 (0.6) × 10^{-1}	28
$Fe(phen)_3^{3+}$	0.98	4.3 (0.7) × 10^{-3}	1.0
$Fe(4,7\text{-}Ph_2\text{-}phen)_3^{3+}$	0.91	1.3 (0.4) × 10^{-3}	0.30

[a] For reduction, vs SCE. [b] Standard deviations in parentheses.

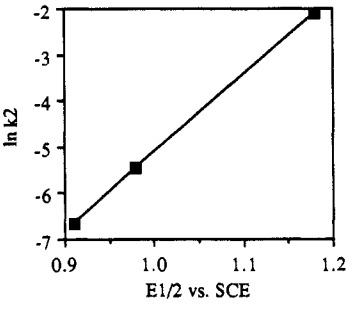

Figure 1. Plot of ln k_2 for oxidation of 1-Me-1,4-CHD (23 °C) vs $E_{1/2}$ of the Fe(III) complex.

In a definitive series of studies, Kochi has demonstrated outer-sphere oxidation of arenes[4,5] and simple olefins[5] by various $Fe(X\text{-phen})_3^{3+}$ species (X-phen = substituted 1,10-phenanthroline) by showing a correlation between the second-order rate constant for substrate oxidation and the difference between the standard oxidation and reduction potentials of the Fe(III) complex and the organic substrate, respectively (ln k_2 vs $E^\circ_{ox} - E^\circ_{red}$), and by demonstrating rate-limiting electron transfer in the overall oxidation process. Using his paradigm, we demonstrated outer-sphere oxidation for a series of simple 1,4-dienes by $Fe(X\text{-phen})_3^{3+}$ (Scheme I).

(1) (a) Schaaf, T. K. *Annu. Rep. Med. Chem.* **1977**, *12*, 182. (b) Bailey, D. M.; Chakrin, L. W. *Annu. Rep. Med. Chem.* **1981**, *16*, 213.

(2) (a) Theorell, H.; Holman, R. T.; Åkeson, Å. *Acta Chem. Scand.* **1947**, *1*, 571. (b) Rosa, M.; Francke, A. *Biochim. Biophys. Acta* **1973**, *327*, 24. (c) Chan, H. W. S. *Biochim. Biophys. Acta* **1973**, *327*, 32. (d) Pistorius, E. K.; Axelrod, B. *J. Biol. Chem.* **1974**, *249*, 3183. (e) de Groot, J. J. M. C.; Veldink, G. A.; Vliegenthart, J. F. G.; Boldingh, J.; Wever, R.; van Gelder, B. F. *Biochim. Biophys. Acta* **1975**, *377*, 71. (f) Greenwald, J. E.; Alexander, M. S.; Fertel, R. H.; Beach, C. A.; Wong, L. K.; Bianchine, J. R. *Biochem. Biophys. Res. Commun.* **1980**, *96*, 817. (g) Slappendel, S.; Malmstrom, B. G.; Petersson, L.; Ehrenberg, A.; Veldink, G. A.; Vliegenthart, J. F. G. *Biochem. Biophys. Res. Commun.* **1982**, *108*, 673.

(3) (a) Corey, E. J.; Cashman, J. R.; Eckrich, T. M.; Corey, D. R. *J. Am. Chem. Soc.* **1985**, *107*, 713. (b) Corey, E. J.; d'Alarcao, M.; Matsuda, S. *Tetrahedron Lett.* **1986**, *27*, 3585. (c) Corey, E. J. *Pure Appl. Chem.* **1987**, *59*, 269 and referenced cited therein. (d) Corey, E. J.; Nagata, R. *Tetrahedron Lett.* **1987**, *28*, 5391. (e) Corey, E. J.; Nagata, R. *J. Am. Chem. Soc.* **1987**, *109*, 8107. (f) Corey, E. J.; Wright, S. W.; Matsuda, S. P. T. *J. Am. Chem. Soc.* **1989**, *111*, 1452.

(4) Fukuzumi, S.; Kochi, J. K. *J. Am. Chem. Soc.* **1982**, *104*, 7599.

(5) (a) Kochi, J. K.; Amatore, C.; Schlesener, C. J. *J. Am. Chem. Soc.* **1984**, *106*, 3567. (b) Schlesener, C. J.; Amatore, C.; Kochi, J. K. *J. Phys. Chem.* **1986**, *90*, 3747.

0002-7863/90/1512-9019$02.50/0